LIMNOLOGY
and
OCEANOGRAPHY

ASLO

Limnol. Oceanogr. 64, 2019, 376–389

doi: 10.1002/lno.11046

Patterns of iron and siderophore distributions across the California Current System

Rene M. Boiteau,[1,2,3] **Claire P. Till**,[4,5] **Tyler H. Coale**,[6] **Jessica N. Fitzsimmons**,[7,8] **Kenneth W. Bruland**,[4] **Daniel J. Repeta**[1*]

[1]Department of Marine Chemistry and Geochemistry, Woods Hole Oceanographic Institution, Woods Hole, Massachusetts
[2]Department of Earth, Atmospheric, and Planetary Sciences, Massachusetts Institute of Technology, Cambridge, Massachusetts
[3]Environmental Molecular Sciences Laboratory, Pacific Northwest National Laboratory, Richland, Washington
[4]Ocean Sciences Department, University of California, Santa Cruz, California
[5]Chemistry Department, Humboldt State University, Arcata, California
[6]Scripps Institution of Oceanography, University of California San Diego, La Jolla, California
[7]Department of Oceanography, Texas A&M University, College Station, Texas
[8]Department of Marine & Coastal Sciences, Rutgers University, New Brunswick, New Jersey

Abstract

Coastal upwelling of nutrients and metals along eastern boundary currents fuels some of the most biologically productive marine ecosystems. Although iron is a main driver of productivity in many of these regions, iron cycling and acquisition by microbes remain poorly constrained, in part due to the unknown composition of organic ligands that keep bioavailable iron in solution. In this study, we investigated organic ligand composition in discrete water samples collected across the highly productive California Coastal upwelling system. Siderophores were observed in distinct nutrient regimes at concentrations ranging from 1 pM to 18 pM. Near the shallow continental shelf, ferrioxamine B was observed in recently upwelled, high chlorophyll surface waters while synechobactins were identified within nepheloid layers at 60–90 m depth. In offshore waters characterized by intermediate chlorophyll, iron, and nitrate concentrations, we found amphibactins and an unknown siderophore with a molecular formula of $C_{33}H_{58}O_8N_5Fe$. Highest concentrations were measured in the photic zone, however, amphibactins were also found in waters as deep as 1500 m. The distribution of siderophores provides evidence for microbial iron deficiency across a range of nutrient regimes and indicates siderophore production and acquisition is an important strategy for biological iron uptake in iron limited coastal systems. Polydisperse humic ligands were also detected throughout the water column and were particularly abundant near the benthic boundary. Our results highlight the fine-scale spatial heterogeneity of metal ligand composition in an upwelling environment and elucidate distinct sources that include biological production and the degradation of organic matter in suboxic waters.

Eastern boundary upwelling systems such as the California Current System (CCS) and the Peru margin are seasonal hotspots of biological activity (Capone and Hutchins 2013). Beginning in the early spring, strong equatorward winds along the coast drive Ekman transport of surface waters offshore (Lynn and Simpson 1987; Strub and James 1995). In their place, cold, salty, nutrient-rich deep waters are upwelled into the euphotic zone where they fuel intense phytoplankton blooms that often persist throughout the spring and summer (Rykaczewski and Checkley 2008; Checkley and Barth 2009). The nitrate, phosphorus, and silicate macronutrients that power these highly productive ecosystems are supplied by the degradation of sinking particulate organic matter, but iron (Fe) is supplied locally from Fe-rich continental shelf sediments (Wheatcroft et al. 1997; Johnson et al. 1999; Bruland et al. 2001; Xu et al. 2002; Berelson et al. 2003; Elrod et al. 2004). Many of the most productive upwelling regions occur along coasts where the shelf is wide and enough dissolved iron (dFe) is supplied by sediments to enable almost complete nitrate, phosphate, and silicate utilization. Iron to nitrate concentration ratios at these sites typically exceed 0.25 nmol/μmol (Elrod et al. 2008; King and Barbeau 2011; Biller and Bruland 2014). However, even in iron replete regions where dFe/N exceed these values, phytoplankton growth and nitrate utilization rates can be stimulated by the addition of readily bioavailable forms of inorganic iron (King and Barbeau 2007),

*Correspondence: drepeta@whoi.edu

Additional Supporting Information may be found in the online version of this article.

highlighting the importance of dissolved Fe (dFe) chemical speciation and bioavailability to biological growth rates and community composition. In regions with narrower shelves where inputs of metals from margin sediments are lower, and offshore where the upper water column is decoupled from sedimentary Fe inputs, upwelled waters have similar concentrations of macronutrients but lower dFe concentrations (Bruland et al. 2008; Biller et al. 2013; Bundy et al. 2014). Under these conditions, the total biomass is limited by the availability of iron, and high concentrations of nitrate and phosphate can persist (King et al. 2012; Biller and Bruland 2014). Nutrient limitation in coastal upwelling regions therefore appears as a mosaic of iron and macronutrient-limited areas determined in part by the delivery of bioavailable iron to surface waters.

Iron limitation in coastal California has been identified using a number of experimental (increase in chlorophyll concentration after iron amendment) and observational (total iron concentration or Fe/N ratio) approaches (King and Barbeau 2007, 2011; Elrod et al. 2008; Biller and Bruland 2014). While these measurements serve as broad indicators of iron stress, they provide little information on what fraction of iron is bioavailable, or how iron is partitioned between bioavailable and non-bioavailable forms. Nearly all soluble iron in marine waters is complexed by organic ligands (Gledhill and Buck 2012). The iron in many of these organic complexes is not directly available to microbes. Under iron stress, some microbes synthesize siderophores, organic compounds with high binding affinity for iron (Vraspir and Butler 2009; Sandy and Butler 2009). The high Fe binding constant of siderophores allows them to extract iron from particulate phases and dissolved organic matter. Siderophore-complexed iron can then be transported into the cell via specific receptor/transporter complexes. The ability to synthesize and take up siderophores is not a characteristic of all marine microbes, so that iron bound to siderophores is available only to members of the microbial community that have the requisite siderophore transporters (Hopkinson and Barbeau 2012).

Direct measurements of siderophores in seawater have only recently become possible (Mawji et al. 2008; Boiteau et al. 2016). Although small in number, these measurements have already shown that a variety of siderophores are present in seawater, and that concentrations are particularly high in regions with low iron, high macronutrient concentrations. Nevertheless, siderophores have also been found in the subtropical North Atlantic and tropical eastern South Pacific Oceans, regions characterized by high-iron concentrations (Mawji et al. 2008; Boiteau et al. 2016). Siderophore production is therefore not restricted to low iron waters. The heterogeneous and dynamic nature of nutrient limitation in the CCS upwelling region therefore makes this an attractive system to explore the coupling between siderophore production and iron cycling.

Here, we report the distribution of siderophores and other organic iron ligands at sites across the CCS. A prior study of organic iron fractions isolated from the CCS by Macrellis et al. (2001) provides support for the presence of siderophores in low iron surface waters in this region. However, direct measurements or identification of siderophores were not yet possible. We quantified and identified ligands using recently developed methods based on liquid chromatography with inductively coupled plasma mass spectrometry and electrospray ionization mass spectrometry (LC-ICPMS-ESIMS) (Boiteau et al. 2016). We found high concentrations of organic iron ligands in near bottom waters over the continental shelf and highly dynamic cycling of siderophores over relatively short spatial/temporal scales throughout the region, even in recently upwelled, high iron waters. Surprisingly, we also found siderophores in a deep-water sample from 1500 m.

Methods

Materials and reagents

High purity solvents and reagents were used, including ultrapure water (18.2 MΩ; qH_2O), liquid chromatography mass spectrometry (LCMS) grade methanol (MeOH) redistilled in a Polytetrafluoroethylene (PTFE) still, and LCMS grade ammonium formate (Optima, Fisher Scientific). Polycarbonate bottles and PTFE tubing for sample collection and solid phase extraction (SPE) were soaked overnight in 0.1% detergent (Citranox), rinsed with qH_2O, and soaked for 1 d in 1 N HCl (trace metal grade, Fisher Scientific) before a final qH_2O rinse. Polypropylene tubes (Nunc, Thermo Scientific) used for sample concentration were washed with qH_2O acidified to pH 2 with hydrochloric acid (HCl, trace metal grade, Fisher Scientific) followed by a final rinse with qH_2O and MeOH prior to use. A 50 μM stock solution of cyanocobalamin (Sigma Aldrich) was prepared in qH_2O. An aqueous solution of iron citrate was prepared by combining 1 mM sodium citrate dihydrate and 100 μM iron (diluted from a 1000 ppm iron reference standard solution, Fisher Scientific).

Sample collection

Samples were collected during the IRNBRU cruise along the CCS between Santa Barbara and the Oregon coast in 2014, an anomalous year in this region due to atypical El Niño wind patterns and reduced upwelling (Fig. 1). Hydrographic data and samples for nitrate analysis were collected using the R/V *Melville* Niskin rosette system fitted with conductivity, depth, temperature, fluorometer, dissolved oxygen, and beam transmission sensors. Nitrate concentrations were analyzed shipboard by flow injection analysis using standard spectrophotometric methods (Parsons et al. 1984).

Water samples (20 L) for ligand analysis were collected using a trace metal clean GeoFish sampling system (Bruland et al. 2005) or PTFE coated GO-Flo bottles deployed on a Kevlar hydroline (Bruland et al. 1979). Concentrations of dFe were determined post-cruise using preconcentration with Nobias-chelate PA1 resin and quantification by ICPMS (Biller and Bruland 2012 as adapted by Parker et al. 2016). For transect surface samples and samples from the Santa Barbara Basin, dFe was

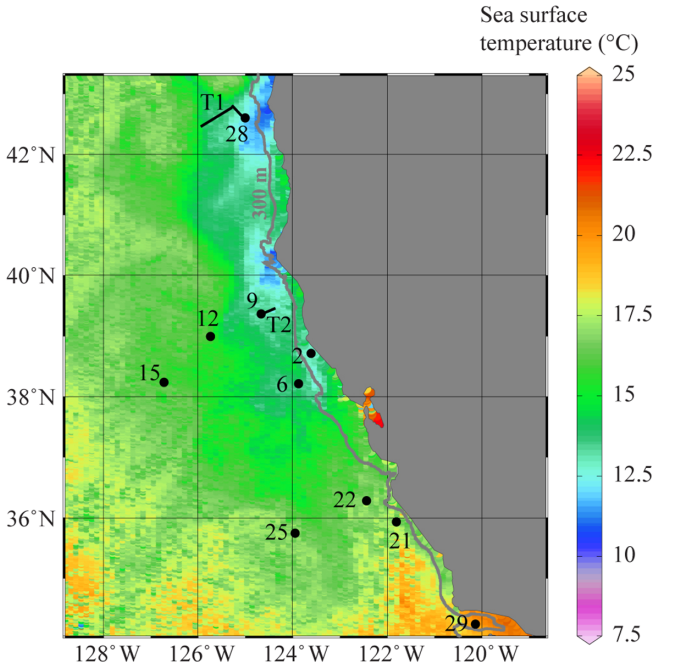

Fig. 1. Map of California coast with sampling stations and transect (T1, T2) locations during the IRNBRU cruise. Sea surface temperature shows the monthly composite for July 2014 from NOAA Polar Orbiting Environmental Satellites Advanced Very High Resolution Radiometer, Local Area Coverage; 300 m bathymetric contour is shown in gray.

determined shipboard using a flow injection based analysis and spectrophotometric detection of iron chelated by N,N-dimethyl-p-phenylenediamine dihydrochloride (Lohan et al. 2006 as adapted by Biller et al. 2013). For ligand analyses, samples were filtered through 0.2 μm polyethersulfone capsule filters into polycarbonate carboys then pumped through SPE resin columns (1 g, ENV) at 15 mL min^{-1} using a peristaltic pump fitted with PTFE and platinum-cured silicone tubing. Immediately before use, SPE columns were conditioned with 5 mL MeOH, rinsed with 10 mL pH 2 qH_2O (acidified with trace metal grade HCl), followed by 10 mL qH_2O. After column loading, columns were rinsed with 10 mL qH_2O to remove salts and frozen onboard. Prior to analysis, samples were thawed, eluted with 10 mL MeOH into 15 mL polypropylene centrifuge tubes, and concentrated in a vacuum rotary centrifuge until only residual water was remaining (< 200 μL). The sample was then transferred to a 1.5 mL microcentrifuge tube and brought to a final volume of 1 mL with qH_2O. Ten microliters of 10 μM cyanocobalamin was added as an internal standard. Samples were analyzed by LC-ICPMS and LC-ESIMS as described below. Total ligands (ligands with and without iron in the original sample) were measured by adding 10 μL of iron citrate solution to 100 μL of sample before LC-ICPMS analyses.

Liquid chromatography

Chromatography was performed on a bioinert Dionex Ultimate 3000 HPLC system fitted with a polyetheretherketone (PEEK) c8 column (3 μm, 2.1 mm × 100 mm, Hamilton Corporation). Seawater extract samples (50 μL injection volume) were separated at a flow rate of 200 μL min^{-1} at 25°C with a 20 min gradient from 90% solvent A (5 mM aqueous ammonium formate) and 10% solvent B (5 mM methanolic ammonium formate) to 90% solvent B, followed by isocratic elution at 90% solvent B for 10 min. A post-column PEEK flow splitter directed 50 μL min^{-1} into the ICPMS or ESIMS.

Liquid chromatography-inductively coupled mass spectrometry

Samples were characterized by LC-ICPMS using a Thermo Scientific iCAP Q quadrupole mass spectrometer equipped with platinum sample and skimmer cones, a perfluoroalkoxy micronebulizer (PFA-ST, Elemental Scientific), and a cyclonic spray chamber cooled to 0°C. Measurements were made in kinetic energy discrimination mode using He collision gas introduced at a rate of 4.2 mL min^{-1} to minimize isobaric ArO^+ interference with ^{56}Fe detection. Isotopes monitored during ICPMS analysis included ^{54}Fe, ^{55}Mn, ^{56}Fe, ^{57}Fe, ^{59}Co, ^{60}Ni, ^{63}Cu, ^{66}Zn, ^{79}Br, and ^{127}I with integration times of 0.05 s. Oxygen gas was introduced to the plasma at 25 mL min^{-1} to prevent the deposition of reduced carbon on the spectrometer's sample and skimmer cones.

To determine iron ligand concentrations, solutions of ferrioxamine E and cyanocobalamin were used to generate a standard calibration curve of ICPMS response to ^{56}Fe. Integration of ICPMS signals and calculation of concentrations were carried out with in-house scripts written in R as described previously (Boiteau et al. 2016). Total ligand concentrations were calculated by integrating the blank-subtracted LCMS signal between 3 min and 32 min and converting peak area to concentration based on the sensitivity for the ferrioxamine E solutions. Siderophore concentrations (e.g., synechobactins) were based on integration of peak areas above a linear baseline connecting the first and last data points of the peak. Signals were normalized based on the area of the cyanocobalamin internal standard (standard deviation of cyanocobalamin peak area was 23% across all analyses). The detection limit (3x background) for ferrioxamine was 5 nM Fe for a 50 μL injection. Since the ICPMS sensitivity decreases as the organic content of the mobile phase increases (40% decrease in sensitivity between 10% and 90% solvent B), this approach underestimates the concentration of compounds that elute after ferrioxamine E (11.1 min) (Boiteau et al. 2013).

Electrospray ionization mass spectrometry

Samples were analyzed by ESIMS by directing the flow from the HPLC into an Orbitrap Fusion mass spectrometer (Thermo Scientific) equipped with a heated ESI source and tuned prior to analysis with ESI calmix (Thermo Scientific). The source parameters were set to a capillary voltage of 3500 V, sheath, auxiliary and sweep gas flow rates of 12, 6, and 2 (arbitrary units), and ion transfer tube and vaporizer temperatures of 300°C and 75°C. Scans were collected in positive mode with

450 K mass resolution. The most abundant ions in each scan were targeted for MS^2 analysis using quadrupole isolation with an m/z = 1 mass window, an ion collection time of 150 ms, a collision energy of 35% in higher-energy collisional dissociation mode, and were detected on the low resolution ion trap mass analyzer.

LC-ESIMS data were analyzed in R after conversion to mzXML file format (MSconvert, proteowizard) (Chambers et al. 2012). A constant time offset was applied to align the retention time of the cyanocobalamin $[M + H]^{2+}$ peak (m/z = 678) with the cyanocobalamin ^{59}Co peak in the LC-ICPMS chromatogram. The isotope pattern matching algorithm described previously (Boiteau and Repeta 2015) was used to identify the masses of iron containing compounds by selecting mass and intensity features from each scan that match the exact mass difference and abundance ratio of ^{56}Fe and ^{54}Fe, and that appear as coherent peaks retention times matching LC-ICPMS peaks (Supporting Information Figs. S1–S9). Structures were determined when possible (Fig. 2; Table 1) based on accurate monoisotopic mass (within 0.002 Da), retention time (within 0.2 min), and MS^2 fragmentation spectra.

Results

Macro and micronutrients across the CCS

LCMS-based ligand characterization paired with nutrient and trace metal measurements were made on 36 seawater samples collected at 10 stations across two surface transects (transects 1 and 2; Fig. 1; Supporting Information Tables S1, S2). Our aim was to track the composition and source of iron binding ligands as waters upwelled over the continental shelf into the photic zone and transited offshore while the microbial community drew down dFe and macronutrients. To this end, we characterized the composition and sources of ligands in water that is upwelled over shallow wide continental shelves (Sta. 2), above suboxic sediments (Sta. 29, Santa Barbara Basin) offshore of narrow shelf regions (Sta. 28), and within the transition zone between the upwelling regions and the California Current (Sta. 6, 9, 12, 15, 21, 22, 25, and transects 1 and 2).

Full water column depth profiles were collected at two stations (Sta. 2 and 29) located inshore of a wide shelf region of the coast (Figs. 3, 4). These sites exhibited intense chlorophyll maxima (> 10 μg L^{-1}) fueled by the upwelling of macronutrients supplied by deep waters as well as dFe supplied by coastal sediments (Biller and Bruland 2013). Station 2 was located just north of San Francisco Bay and had a water column depth of 106 m. At the time of sampling, this site was characterized by cold surface waters (10°C) with high concentrations of chlorophyll (10.3 μg L^{-1}), nitrate (16 μM), phosphate (1.4 μM), and dFe (2.8 nM), reflecting the recent upwelling of nutrient rich deep water. Elevated concentrations of dFe were observed near the sediment-water interface, reaching 16.5 nM at 90 m. A decrease in beam transmission was observed at 60 m and 90 m, indicating lateral advection of two subsurface plumes of resuspended sediments (Fig. 3).

Station 29, located in the Santa Barbara basin (Fig. 4), had a warm mixed layer (18.2°C) with very low nitrate (< 0.02 μM) and high dFe (4.6 nM) concentrations overlying an intense subsurface chlorophyll maximum (14.9 μg L^{-1}) located within a sharp thermocline at 21 m with elevated dissolved nitrate (5.3 μM) and phosphate (0.5 μM) concentrations. Like Sta. 2, sediments are a major source of dFe to the photic zone at this location (John et al. 2012). DFe concentrations were significantly elevated within the suboxic zone (O_2 < 2 μmolM kg^{-1}) below the basin sill depth at 530 m. DFe reached a maximum concentration (> 50 nM) near the sediment interface (580 m).

We also sampled an upwelling site (Sta. 28) located in deep water (1200 m) off the narrow shelf region of the Oregon coast (Fig. 5). Surface temperature (10.9°C) and nitrate concentrations (17.0 μM) were similar to those measured along the wide shelf region at Sta. 2. However, chlorophyll a (Chl *a*) concentrations were notably lower with a maximum of only 2 μg L^{-1} at the subsurface chlorophyll maximum. The absence of benthic iron inputs was reflected in the significantly lower dFe concentrations at the surface (0.7 nM) and throughout the upper water column (1.6–3.0 nM to 300 m).

Finally, samples were collected across the transition zone between cold saline upwelled waters and the warm oligotrophic offshore waters of the CCS (Sta. 6, 9, 12, 15, 21, 22, and 25, Supporting Information Table S1). These regions are

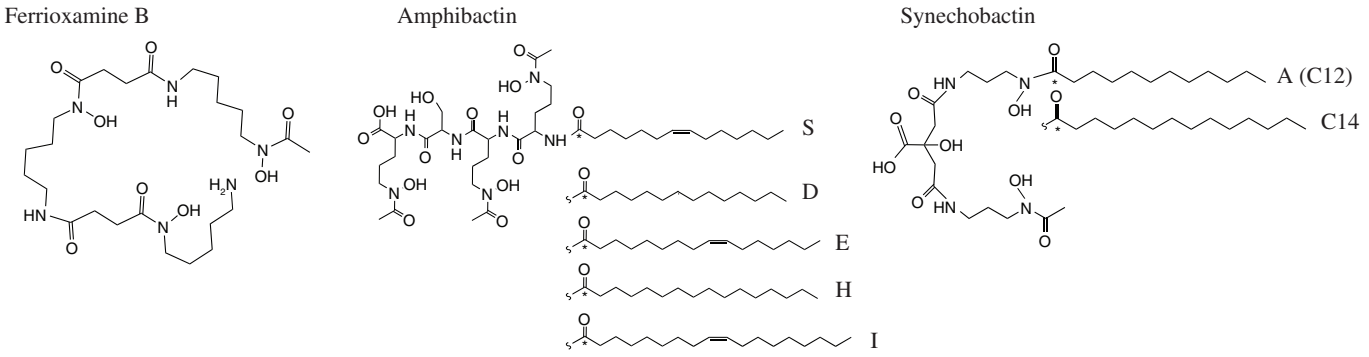

Fig. 2. Molecular structures of siderophores identified across the CCS.

Table 1. Identification of iron binding compounds in CCS seawater.

Elution time (min)	^{56}Fe monoisotopic $[M + H]^+$ *m/z*	Molecular formula	Identity	Major MS/MS fragments detected (*m/z*)
12.5	614.273	$C_{25}H_{46}O_8N_6Fe^+$	Ferrioxamine B	397, 414, 468, 496
19.4	614.261	$C_{26}H_{46}O_9N_4Fe^+$	Synechobactin A (C12)	206, 288, 298, 458, 484, 500, 550, 568, 578
21.1	642.292	$C_{28}H_{50}O_9N_4Fe^+$	Synechobactin C14	206, 288, 298, 486, 512, 528, 578, 596, 606
22.9	709.371	$C_{33}H_{59}O_8N_5Fe^{+*}$	Unknown	477, 577, 594, 648, 691
19.7	883.399	$C_{38}H_{65}O_{13}N_7Fe^+$	Amphibactin S	485, 578, 606, 651
20.5	885.415	$C_{38}H_{67}O_{13}N_7Fe^+$	Amphibactin D	485, 580, 608
21.1	911.43	$C_{40}H_{69}O_{13}N_7Fe^+$	Amphibactin E	485, 606, 634
21.9	913.446	$C_{40}H_{71}O_{13}N_7Fe^+$	Amphibactin H	485, 636
22.2	939.462	$C_{42}H_{73}O_{13}N_7Fe^+$	Amphibactin I	485, 634, 662

*Hypothesized chemical formula.

characterized by complex patterns of seaward jets, filaments, and mesoscale eddies (Checkley and Barth 2009), with warm (> 12°C) surface waters and intermediate chlorophyll levels (0.5–3 μg L^{-1}). Surface dFe concentrations were consistently low (0.03–0.36 nM), while surface nitrate concentrations were variable (0.2 nM up to 20 nM) due to different degrees of biological nutrient drawdown and resupply by eddy driven upwelling. Such high nitrate, low chlorophyll conditions imply that low concentrations of dFe limited the rate of biological macronutrient uptake throughout most of this region.

Iron ligands at wide shelf upwelling Sta. 2 and 29

In the high chlorophyll surface samples collected at Sta. 2 (Fig. 3), LCMS revealed trace amounts of two iron-ligand complexes (FeLs). The FeL eluting at 12 min (Fig. 3, peak a) and was identified as ferrioxamine B based on co-elution with authentic ferrioxamine B, and the detection of the ^{56}Fe isotopologue (614.273 *m/z*) by LC-ESIMS. We were unable to detect an ion at *m/z* 612.278 from the ^{54}Fe isotopologue due to isobaric interferences from coeluting species at this retention time (Supporting Information Fig. S1). A second Fe containing compound was detected at 8 min, but a corresponding pair of iron-ligand isotopologues likewise could not be detected by ESIMS.

Samples collected within the nepheloid layers at 60 m and 90 m each displayed two prominent iron ligands eluting at 19 min and 21 min (Fig. 3, peaks b and c). A pair of coeluting ions matching the iron isotope pattern was identified in the LC-ESIMS spectra for each of these peaks, with ^{56}Fe monosotopic masses of 614.261 *m/z* and 642.292 *m/z*, respectively (Supporting Information Figs. S2, S3). Tandem MS/MS analyses of these ions yielded diagnostic fragments for synechobactin C12 (synechobactin A) and synechobactin C14, respectively, including neutral losses of 46.006 ($-CH_2O_2$), 113.996 ($-C_4H_2O_4$), 130.027 ($-C_5H_6O$), and 156.006 ($-C_6H_4O_5$), consistent with previous mass spectra of synechobactins (Boiteau and Repeta 2015). These identities were confirmed by comparison with retention time, mass, and MS^2 spectra of authentic synechobactin standards isolated from iron-limited cultures of *Synechococcus* sp. PCC 7002. The concentrations of these siderophores were 18 pM and 12 pM at 60 m and 80 m, respectively. These concentrations represent a conservative estimate, since extraction efficiencies for synechobactins by SPE are < 100%.

In addition to ferrioxamine and synechobactin siderophores, a distinctive broad peak of unresolved polar ^{56}Fe compounds eluting between 4 min and 20 min was detected the chromatogram of all samples. The intensity of this peak increased with depth. In surface waters, we noted the presence of a second broad peak eluting between 20 min and 25 min. Both peaks represent a complex and diverse suite of iron containing organic ligands that elute over a wide range of retention times. We suspect that these ligands are humic-like substances that arise from the degradation of microbial-derived organic matter in the water column and in sediments. At Sta. 2, the sum of all FeL extracted increased from ~ 123 pM in surface waters to 301 pM at 90 m, with the decrease in nonpolar ligands being more than offset by the increase in polar FeL at depth (Fig. 3, Supporting Information Table S2).

A greater than 10-fold excess (relative to total ligands) of ferric citrate was added to splits of all samples to saturate "excess" ligands that were not complexed to iron in our original sample (Fig. 3). Station 2 siderophores were fully saturated with iron (we measured no increase in ligand concentration after addition of Fe-citrate), which is consistent with their strong iron binding stability constants and the high dFe concentration (> 3 nM) at this site. However, we measured significant increases of between 26% and 72% in iron associated with polar humic substances (retention time 4–20 min).

No discrete ligands were observed in any sample collected at the Santa Barbara Basin Station 29 (Fig. 4). Concentrations of ligands attributed to humic substances in surface waters (~ 110 pM) were similar to values measured at Sta. 2, but increased sharply in the suboxic portion of the water column, reaching ~ 900 pM in our deepest sample at 570 m. Addition of ferric citrate more than doubled the amount of

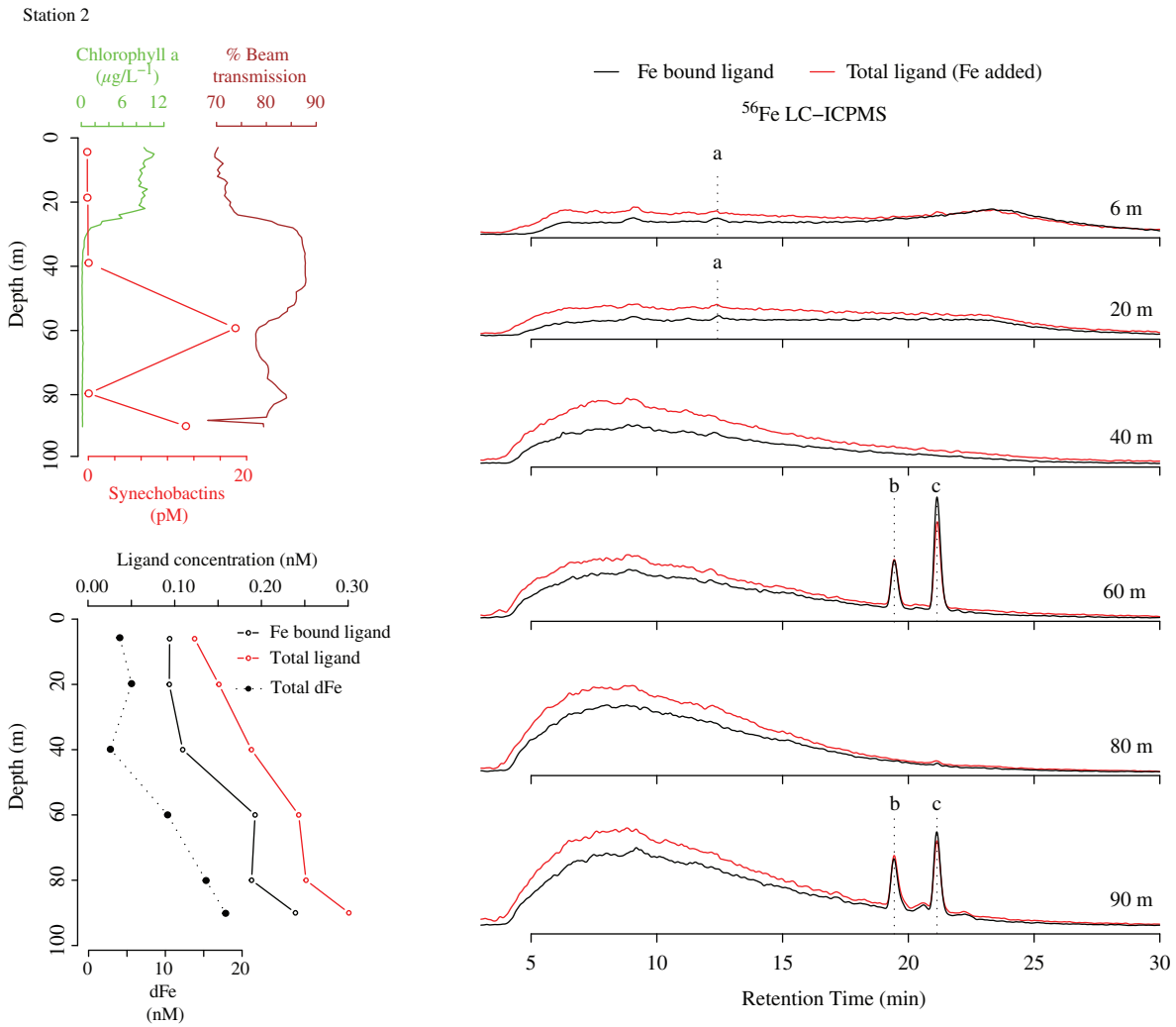

Fig. 3. Wide shelf upwelling region (Sta. 2). (Left) Depth profiles of Chl *a*, beam transmission, dissolved iron, and LC-ICPMS-based FeL concentrations. (Right) ^{56}Fe LC-ICPMS chromatograms of organic extracts collected from each depth. Dashed lines indicate chromatographic peaks from compounds that were identified by LC-ESIMS. LC-ESIMS (a) ferrioxamine B (b) synechobactin C12, and (c) synechobactin C14.

iron associated with humic substances in samples at and shallower than 200 m, but had little effect on total ligands in the deepest 550 m and 570 m samples in the suboxic water column.

Iron ligands at narrow shelf upwelling Sta. 28

We collected two samples for ligand characterization at Sta. 28 from the mixed layer (15 m) and deep chlorophyll maximum (DCM; 42 m). DFe concentrations in both samples were relatively low (Fig. 5; 0.72 nM and 0.53 nM, respectively). Concentrations of Fe associated with chromatographically unresolved ligands attributed to humic substances (191–264 pM) were comparable to Fe-humic ligand concentrations recovered by SPE at the shallow wide shelf sites. We detected no siderophores in either sample by LC-ICPMS. Addition of ferric citrate increased the amount of FeL by 24–142% (Fig. 4).

Iron ligands in transition region waters

Nonpolar iron binding compounds with retention times between 19 min and 24 min were detected in 19 out of 23 samples. Compounds eluting at 19.7 min, 20.5 min, 21.1 min, 21.9 min, and 22.2 min were identified as amphibactins S, D E, H, and I (Supporting Information Figs. S4–S8). We were able to detect co-eluting ^{54}Fe and ^{56}Fe isotopologue ions for each compound, and MS^2 spectra for each molecular ion showed diagnostic neutral losses of *m/z* 218 ($C_8H_{14}N_2O_5$), 277 ($C_{10}H_{19}N_3O_6$), and 305 ($C_{11}H_{19}N_3O_7$). Retention times matched amphibactin standards isolated from the marine bacterium *Vibrio cyclitrophicus* 1F-53 (Boiteau et al. 2016). These amphiphilic siderophores are composed of a polar iron binding head group and a fatty acid side chain of variable length. The most abundant amphibactins were consistently S, E, and I, which all possess a single unsaturation in the fatty acid side chain. Their concentrations in the

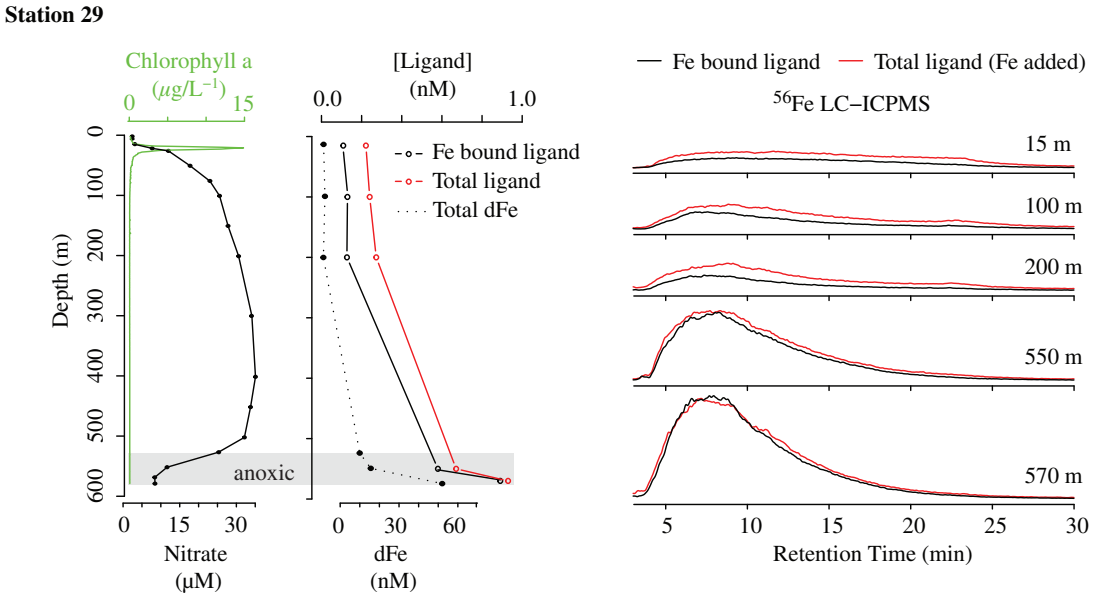

Fig. 4. Santa Barbara basin (Sta. 29). (Left) Depth profiles of Chl *a*, nitrate, dissolved iron, and LC-ICPMS based FeL concentrations. (Right) ^{56}Fe LC-ICPMS chromatograms of organic extracts collected from each depth.

transition zone stations are summarized in Supporting Information Table S1 and ranged from 0.9 pM to 6.4 pM.

Another discrete nonpolar peak at 22.9 min was observed by LC-ICPMS in seven samples from the transition region (Supporting Information Fig. S10). We detected both ^{54}Fe and ^{56}Fe isotopologues (707.376 *m/z* and 709.371 *m/z*, respectively) of this compound (siderophore-709) by LC-ESIMS. By assuming that the compound contains only CHNO, we were able to determine a molecular formula of $C_{33}H_{59}O_8N_5Fe^+$ as the only match within 1 ppm error of the measured mass. This compound does not match the mass or formula of any known siderophore published in siderophore libraries (Hider and Kong 2010; Baars et al. 2014) or any biological molecule in the PubChem database (Kim et al. 2016). Based on the late retention time and low heteroatom content of this molecule, it appears to have similar amphiphilic character as the amphibactins.

The occurrence and abundance of amphibactins were highly variable in space and time. This is well illustrated by the appearance of amphibactins and siderophore-709 across several eddies in the transition zone (Supporting Information Figs. S10, S11). We collected samples from the central mixed layer and DCM of two cyclonic eddies (Sta. 9 and 15), and from the edge of one anticyclonic eddy (Sta. 12) from 11 July to 12 July, and then returned to sample surface waters across the eddy centered at Sta. 9 on 13 July (Fig. 6). The eastern eddy (Sta. 9) was composed of recently upwelled water and had relatively high nitrate concentrations (5.2 μM), although dFe was depleted (< 0.2 nM). In this eddy, amphibactins were found at high concentrations in the surface (5.1 pM), and

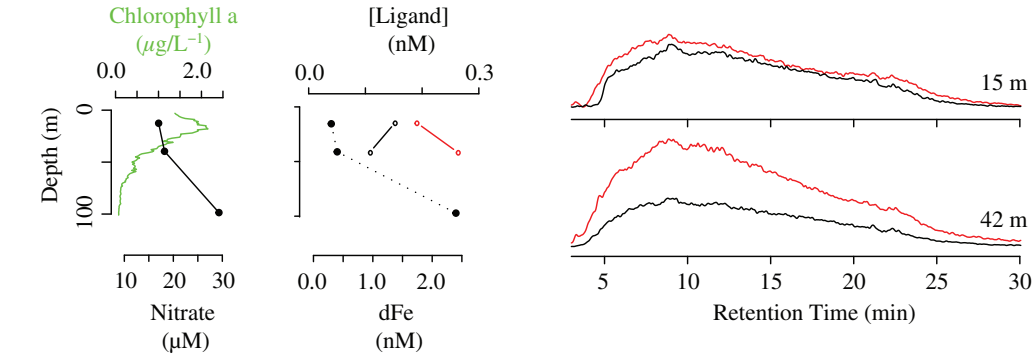

Fig. 5. Narrow shelf upwelling region (Sta. 28). (Left) Depth profiles of Chl *a*, nitrate, dissolved iron, and LC-ICPMS-based FeL concentrations. (Right) ^{56}Fe LC-ICPMS chromatograms of organic extracts collected from each depth.

lower concentrations at the DCM (4.0 pM). Farther offshore, the westward cyclonic eddy (Sta. 15) was composed of warmer water that had spent more time at the surface and was significantly depleted in both nitrate and iron. Here, amphibactin concentrations were lower (4.3 pM) at the surface and below detection in the DCM. The anticyclonic eddy (Sta. 12) was characterized by a deeper nutricline and warm, lower salinity water that likely originated from the California Current. Amphibactin concentrations were low in the nitrate and iron depleted surface waters (1.6 pM). Just above the nutricline in the DCM (48 m), amphibactins appeared at high concentrations (6.4 pM).

Amphibactins were also found at low concentrations (2.9 pM) in a sample collected from 1500 m (Sta. 12). Upon returning to the eastern eddy and Sta. 9, we collected samples every hour as we crossed the eddy to investigate the fine scale distribution of siderophores (transect 1). A longer chromatographic gradient was used to better resolve amphibactins by LC-ICPMS (Fig. 6). Siderophore-709 was the most abundant iron compound detected across the high chlorophyll western side and center of the eddy. Toward the eastern edge, amphibactins were more abundant, mirroring our observations from Sta. 9 several days earlier. Similar tradeoffs between Siderophore-709 and amphibactins were observed across a transect in the transition zone west of Sta. 28 (transect 2). This fine scale heterogeneity demonstrates that mesoscale features across the CCS transition zone have a strong impact on siderophore distributions.

Total solid phase extractable ligand concentrations were similar across most samples in the transition zone, between 0.16 nM and 0.31 nM. Deep samples consistently contained higher concentrations of ligands than surface samples, and most Fe was associated with unresolved humic substances. Addition of iron to the SPE extract increased the total amount of SPE extractable Fe ligand detected by 10–70%.

Discussion

Distribution of siderophores across the CCS

We measured large changes in the concentration and distributions of siderophores across the CCS, even over small spatial and temporal scales. These changes suggest that siderophores are highly dynamic reporters of microbe-iron interactions. Distinct classes of siderophores were observed in particular nutrient regimes defined by dissolved nitrate, iron, and chlorophyll concentrations (Fig. 7). Ferrioxamine B was characteristic of surface samples with high concentrations of Chl *a* (> 10 μg mL^{-1}), nitrate, and dFe, while amphibactins were most common in offshore waters with variable concentrations of nitrate, but where dFe and chlorophyll concentrations were low. Siderophore-709 was also common offshore, although its distribution was quite distinct from the amphibactins, as exemplified by the fluctuations between the siderophore 709 and amphibactins across the cyclonic eddy (Fig. 6).

These generalized patterns of siderophore distributions are similar to those observed in other regions of the ocean. In the eastern tropical South Pacific (GEOTRACES GP16), ferrioxamine B was similarly the most abundant siderophore detected in high dFe, high nitrate upwelling waters near the Peru coast, while high concentrations of amphibactins were similarly found in offshore waters with low dissolved iron (< 0.2 nM) but high nitrate concentrations (Boiteau et al., 2016). In the eastern

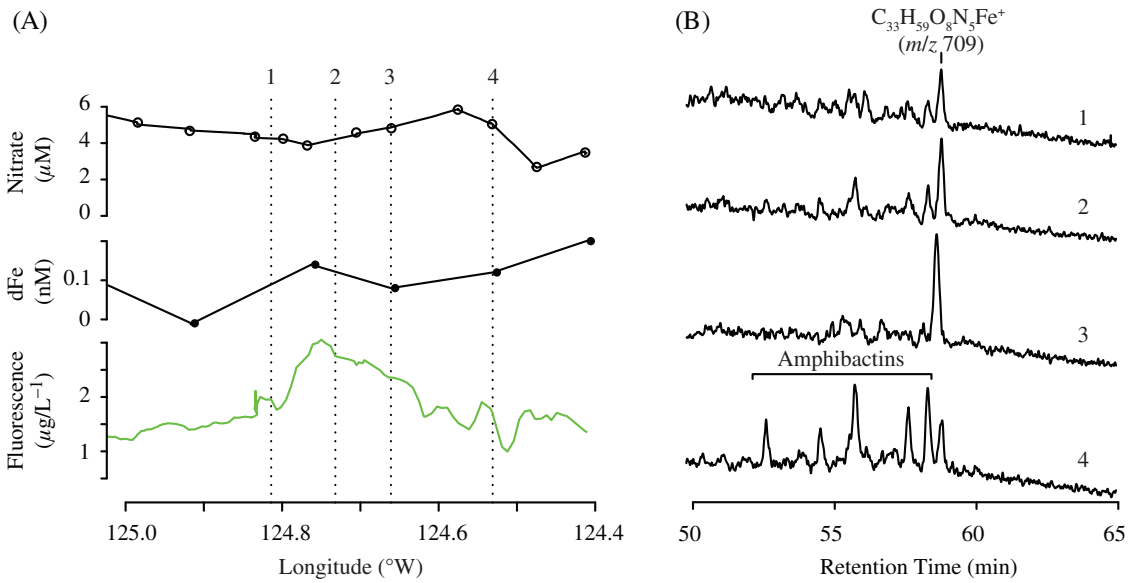

Fig. 6. (**A**) Surface (3 m) profiles of underway nitrate, dFe, and fluorescence across a cyclonic eddy (T2). Location of LC-ICPMS samples 1–4 indicated by dashed lines. (**B**) LC-ICPMS chromatograms of ^{56}Fe from samples collected across the eddy field of transect 1. A chromatographic gradient from 5% to 95% solvent B over 60 min was used to better resolve the amphibactin peaks.

tropical South Pacific, siderophore-709 was found to co-occur with amphibactins, but again, its abundance was not clearly coupled to amphibactin concentrations. Siderophore 709 and amphibactins may be synthesized by different microbes that inhabit similar oceanographic regimes, but have slightly different dynamics or responses to nutrient availability. In contrast, a siderophore of mass 959.430 *m/z* was abundant in the tropical Pacific (Boiteau et al. 2016), but not detected in any of our samples from the CCS.

In the subtropical North Pacific near Hawaii, ferrioxamine E was detected in low nitrate, low iron surface waters and the DCM rather than in high nitrate high iron waters, while amphibactins were also detected below 200 m depth where dFe was < 0.1 nM but dissolved nitrate was > 0.5 μM (Bundy et al. 2018), similar to this study. Finally, Mawji et al. (2008) detected only ferrioxamines E and G in surface waters across the North Atlantic, which has higher dFe concentrations (> 0.3 nM) compared to the CCS transition zone and tropical Pacific HNLC region. However, when surface waters were amended with various carbon substrates to iron limit the heterotrophic community, amphibactins were produced (Gledhill et al. 2004; Mawji et al. 2008, 2011). Even when amphibactin-producing bacteria are present, amphibactins have only been found in waters with low iron concentrations (< 0.3 nM).

Synechobactins were observed in samples characterized by very low chlorophyll fluorescence and high dissolved iron concentrations (Fig. 7), and may have been associated with nepheloid layers advected from the shelf inshore. It is possible that the synechobactins we measured at Sta. 2 were produced by microbes growing on the seafloor that were suspended by turbulent mixing within the benthic boundary. High concentrations of synechobactins at 60 m and 90 m but the near absence of synechobactins at 80 m are consistent with this explanation. However, synechobactins could have been produced at 60 m and 90 m due to local factors that stimulated microbial iron demand. Under either scenario, the high concentrations of these siderophores implies that iron bioavailability was low in the nepheloid layer or in surface sediments despite high dFe concentrations, thus incentivizing microbes to expend energy and resources on siderophore secretion to facilitate uptake. Currently known synechobactin producers are cyanobacteria. They include the cyanobacteria *Synechococcus* sp. PCC 7002, which was isolated from marine muds (Ito and Butler 2005; Boiteau and Repeta 2015) and the nitrogen fixing cyanobacteria *Anabaena variabilis* (Deicke et al. 2014). The freshwater cyanobacterium *Nostoc* sp. PCC7120 also harbors genes for the synechobactin biosynthetic pathway. However, this does not preclude the possibility that non-photoautotrophic organisms can also produce these compounds, and the low chlorophyll concentrations between 60 m and 90 m (< 0.3 μg L^{-1}) suggest that little photosynthesis occurs at these depths.

Humic ligands and iron from the benthic boundary

SPE retains a highly complex mixture of nonpolar, dissolved organic constituents. Even state-of-the-art reverse phase chromatographic separations do not resolve these mixtures, which appear in chromatographic traces as broad, unresolved baselines of fluctuating intensities. These chromatographically

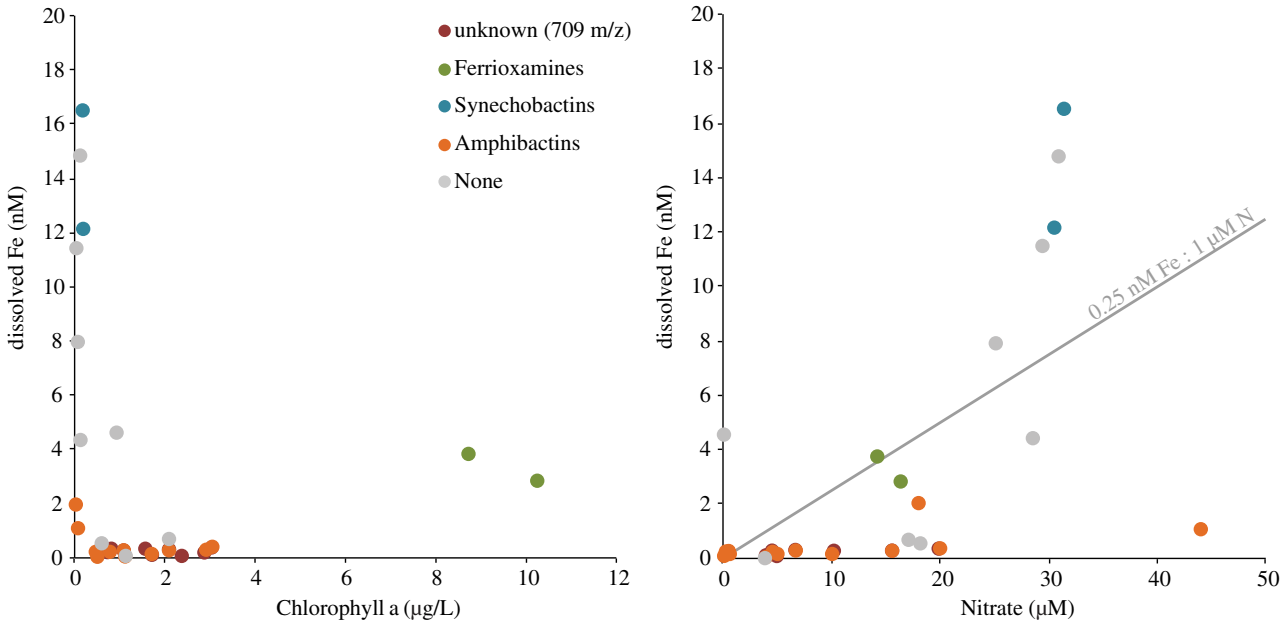

Fig. 7. Oceanographic conditions where siderophores were detected across the CCS. Gray line corresponds to the Fe : N ratio typical of marine diatoms (Elrod et al. 2008).

unresolved compounds, likely substances formed during organic matter degradation, were the most abundant and persistent ligands detected by LC-ICPMS. At all stations sampled for this study, concentrations of SPE ligands increased with depth, consistent with a sedimentary source and surface water sink. Although dissolved organic carbon (DOC) concentrations do not rise significantly at the sediment-water boundary (Hansell et al. 1995; Burdige et al. 1999) sediments do contribute colored and fluorescent dissolved organic matter, some of which may complex iron, to the water column (Clark et al. 2008). We noted high concentrations of iron-ligand complexes at Santa Barbara Basin Station 29, particularly in the suboxic waters below 500 m, within a region characterized by a significant flux of radiocarbon-depleted, refractory DOC to the overlying water column (Burdige et al. 2016).

The SPE humic substances from near the benthic boundary were saturated with iron, consistent with the benthic boundary as a source of ligands that stabilize sedimentary iron in a soluble form that is upwelled to surface waters. Electrochemical techniques have similarly suggested that humic substances are important ligands for iron in marine systems (Laglera and van den Berg 2009; Mahmood et al. 2015), and that they are released from shallow sediments along the continental shelf near San Francisco Bay (Bundy et al. 2014). These ligands had conditional stability constants (log $K^{cond}_{FeL,L'}$) that were weaker than siderophores, ranging from 11.2 to 11.9. A portion of these ligands (estimated at 3–18%) were potentially composed of terrestrially derived humic substances (Bundy et al. 2014, 2015), with the balance contributed by autochthonous marine humic substances (Hertkorn et al. 2015; Repeta 2015). Concentrations of humic substances estimated by electrochemical measurements in seawater were > 1 nM (Laglera and van den Berg 2009; Bundy et al. 2014, 2015). It is likely that some these ligands are not retained during the SPE, resulting in lower concentrations detected by LCMS in this study. The specific characteristics and relative contribution of humic ligands from sediments, terrestrial input, and the water column production to the CCS is unknown, but may influence water column iron cycling in this region.

Humic ligands bind iron more weakly than siderophores and thus buffer a significantly larger pool of bioavailable free iron. If concentrations of humic-bound iron are large enough and dissociation kinetics are fast enough, then microbes can rely on a small but constantly replenished supply of free iron that can be taken up directly (Morel et al. 2008). However, if this pathway is insufficient to sustain maximum growth rates and the organism becomes iron stressed, additional iron acquisition pathways, such as siderophore production/uptake must be utilized. Further work is needed to elucidate the kinetics of dissociation and uptake of iron associated with these humic ligands.

Siderophores as indicators of microbial iron stress

Despite a lengthy history of research on iron cycling across the CCS as a prototypical coastal upwelling system, the extent to which iron deficiency impacts biological community composition and growth still remains unclear. One commonly used metric of iron limitation is the ratio of dFe to dissolved macronutrients compared to the average elemental stoichiometry commonly found in microorganisms (Elrod et al. 2008; King and Barbeau 2011; Biller and Bruland 2014). For example, Elrod et al. (2008) suggested that diatoms were susceptible to iron limitation in regions of the CCS exhibiting Fe:NO_3^- ratios below this value based on typical growth requirements (Fe/N ~ 0.25 nmol/μmol). Since Fe:NO_3^- is easily measured, this approach provides a useful estimate of the regional extent of iron limitation in diatoms. However, these estimates are inherently conservative; while most of the measured nitrate will eventually be taken up by organisms, much of the dissolved iron that reaches the surface ocean is removed by scavenging processes rather than biological uptake. Furthermore, these ratios are coarse estimates of nutrient quotas that can vary significantly in nature (Marchetti and Maldonado 2016).

A more direct means of evaluating iron limitation is to perform incubation experiments with added ferric iron and observe changes in microbial community composition, chlorophyll fluorescence, or rates of macronutrient uptake. Iron amendment experiments in the CCS have revealed that iron uptake rates can limit overall growth even when ambient iron concentrations appear to be sufficient based on total iron to dissolved macronutrient to ratios (King and Barbeau 2007). These observations imply that much of the dissolved iron present in the CCS is not readily available to the microbes. Therefore, assessments of limitation that rely on measurements of total dFe concentration may not fully capture the breath of conditions under which iron limits microbial community production. Measurements of siderophore distribution and abundance may provide another means of making these assessments. To avoid unnecessary expenditure of energy and nutrients, siderophore biosynthesis is tightly controlled by transcription factors that respond to changes in intracellular iron concentrations (Miethke and Marahiel 2007; Tunca et al. 2007). When the supply of iron in readily available forms such as inorganic Fe(II) or Fe(III) is too low to fulfill cellular quotas, siderophore production and uptake is activated in an effort to alleviate iron limitation. Thus siderophore production is directly correlated with the stress response of the producer to iron deficiency. The presence of very high concentrations of amphibactins across the canonically iron limited transition zone is one clear example this coupling between iron stress and siderophore production in the environment. In other cases, we detected siderophores in regions where iron limitation was not expected based on dFe/N ratios exceeding 0.25 nmol/μmol, and absolute dFe concentrations as high as 16 nM (Fig. 7). These results suggest that iron limitation may be more widespread than previously thought.

The distribution of siderophore biosynthesis and uptake genes across bacterial genera is often patchy, such that it is not possible to attribute their production to a single taxon.

Currently known producers of amphibactins include a wide range of bacteria that occupy distinct environmental niches, including several copiotrophic *Vibrio* taxa, the oil degrading marine bacteria *Alcanivorax borkumensis*, the ammonium oxidizing bacteria *Nitrosococcus halophilus,* and the nitrogen fixing bacteria *Azotobacter chroococcum* (Martinez et al. 2003; Kem et al. 2014; Boiteau et al. 2016; Baars et al. 2017). While the dispersion of siderophore biosynthesis pathways makes it challenging to identify specific producers in the environment, it suggests that iron deficiency exerts an evolutionary selection pressure that promotes the dissemination of siderophore biosynthesis and uptake genes. Siderophore utilization is a trait which is even more widespread, and observed in siderophore producing bacteria, bacteria that do not produce siderophores, and in eukaryotic phytoplankton (Hider and Kong 2010). Future work combining siderophore detection by LCMS with metagenomic and single cell genomic analyses will provide greater insight into the major producers of these compounds in the marine environment.

There are hundreds of known siderophores which differ in their chemical structure, synthesis pathway, the amount of metabolic energy expended in synthesis, strength of iron complexation, solubility in seawater, and elemental composition (e.g., some siderophores are N rich, while others are not). We expect all of these differences will impact the effectiveness of any siderophore in facilitating iron uptake from seawater. Determining which of these factors are most important, and the ecological advantage of using a particular siderophore over others will require more detailed studies on the chemical properties of the siderophores and the lifestyles of their producers and consumers. Our measurements from the CCS, along with the handful of other siderophore measurement made in the North Atlantic and South Pacific oceans suggest that ferrioxamines, which form unusually strong iron complexes, are particularly advantageous in upwelling systems and at other high iron sites where inputs of strongly complexed iron from dust or sedimentary organic matter are important. Amphibactins, which form less strong iron complexes, but are more lipophilic, appear to offer some advantage in systems which have lower iron, but where iron may be bound less strongly by competing ligands. Finally, photo-reactive siderophores such as synechobactins may be preferentially produced within benthic waters where they are less susceptible to degradation by sunlight.

Conclusions

Despite the importance of organic ligands to the supply of iron in coastal upwelling regions of the ocean, the chemical nature, sources, and bioavailability of these ligands is still poorly constrained. This study demonstrates that siderophores and humic ligands both play a role in iron cycling across the CCS. Ferrioxamine and amphibactin siderophores were present in many areas of the CCS, and their composition was found to vary across different nutrient regimes. Relative to amphibactins, ferrioxamines were more abundant in recently upwelled, higher dFe waters, while amphibactins were more typically associated with low dFe waters with low dFe/nitrate ratios. The overall trends in ferrioxamine and amphibactin distributions within the CCS matched those observed previously in the South Pacific. However, discrete sampling revealed significant variability over relatively short spatial and temporal scales. We also measured high concentrations of amphibactins in two subsurface samples at 118 m and 1500 m that had relatively high dFe concentrations. Additionally, high concentrations of synechobactins were also measured in two subsurface samples that appeared to be associated with nepheloid layers near the benthic boundary. Iron that is sourced from sediments is largely chelated by highly heterogeneous ligands likely formed from decomposing organic matter on the seafloor. Our data suggest that these ligands persist in surface waters, although the amount of iron associated with them decreases as dFe decreased due to biological uptake or scavenging. Overall, these findings demonstrate numerous distinct sources of iron-binding ligands of varied composition to the surface ocean that give rise to a dynamic and heterogeneous ligand pool across the CCS.

References

Baars, O., F. M. M. Morel, and D. H. Perlman. 2014. ChelomEx: Isotope-assisted discovery of metal chelates in complex media using high-resolution LC-MS. Anal. Chem. **86**: 11298–11305. doi:10.1021/ac503000e

Baars, O., X. Zhang, M. I. Gibson, A. T. Stone, F. M. M. Morel, and M. R. Seyedsayamdost. 2017. Crochelins: Siderophores with an unprecedented iron-chelating moiety from the nitrogen-fixing bacterium *Azotobacter chroococcum*. Angew. Chem. Int. Ed. **57**: 536–541. doi:10.1002/anie.201709720

Berelson, W. and others 2003. A time series of benthic flux measurements from Monterey Bay, CA. Cont. Shelf Res. **23**: 457–481. doi:10.1016/S0278-4343(03)00009-8

Biller, D. V., and K. W. Bruland. 2012. Analysis of Mn, Fe, Co, Ni, Cu, Zn, Cd, and Pb in seawater using the Nobias-chelate PA1 resin and magnetic sector inductively coupled plasma mass spectrometry (ICP-MS). Mar. Chem. **130–131**: 12–20. doi:10.1016/j.marchem.2011.12.001

Biller, D. V., and K. W. Bruland. 2013. Sources and distributions of Mn, Fe, Co, Ni, Cu, Zn, and Cd relative to macronutrients along the Central California coast during the spring and summer upwelling season. Mar. Chem. **155**: 50–70. doi:10.1016/j.marchem.2013.06.003

Biller, D. V., T. H. Coale, R. C. Till, G. J. Smith, and K. W. Bruland. 2013. Coastal iron and nitrate distributions during the spring and summer upwelling season in the Central California Current upwelling regime. Cont. Shelf Res. **66**: 58–72. doi:10.1016/j.csr.2013.07.003

Biller, D. V., and K. W. Bruland. 2014. The central California Current transition zone: A broad region exhibiting

evidence for iron limitation. Prog. Oceanogr. **120**: 370–382. doi:10.1016/j.pocean.2013.11.002

Boiteau, R. M., J. N. Fitzsimmons, D. J. Repeta, and E. A. Boyle. 2013. Detection of iron ligands in seawater and marine cyanobacteria cultures by high-performance liquid chromatography-inductively coupled plasma-mass spectrometry. Anal. Chem. **85**: 4357–4362. doi:10.1021/ac3034568

Boiteau, R. M., and D. J. Repeta. 2015. An extended siderophore suite from *Synechococcus* sp. PCC 7002 revealed by LC-ICPMS-ESIMS. Metallomics **7**: 877–884. doi:10.1039/C5MT00005J

Boiteau, R. M. and others 2016. Siderophore-based microbial adaptations to iron scarcity across the eastern Pacific Ocean. Proc. Natl. Acad. Sci. USA **113**: 14237–14242. doi:10.1073/pnas.1608594113

Bruland, K. W., R. P. Franks, G. A. Knauer, and J. H. Martin. 1979. Sampling and analytical methods for the determination of copper, cadmium, zinc, and nickel at the nanogram per liter level in sea water. Anal. Chim. Acta **105**: 233–245. doi:10.1016/S0003-2670(01)83754-5

Bruland, K. W., E. L. Rue, and G. J. Smith. 2001. Iron and macronutrients in California coastal upwelling regimes: Implications for diatom blooms. Limnol. Oceanogr. **46**: 1661–1674. doi:10.4319/lo.2001.46.7.1661

Bruland, K. W., E. L. Rue, G. J. Smith, and G. R. DiTullio. 2005. Iron, macronutrients and diatom blooms in the Peru upwelling regime: Brown and blue waters of Peru. Mar. Chem. **93**: 81–103. doi:10.1016/j.marchem.2004.06.011

Bruland, K. W., M. C. Lohan, A. M. Aguilar-Islas, G. J. Smith, B. Sohst, and A. Baptista. 2008. Factors influencing the chemistry of the near-field Columbia River plume: Nitrate, silicic acid, dissolved Fe, and dissolved Mn. J. Geophys. Res. **113**: 1–23. doi:10.1029/2007JC004702

Bundy, R. M., D. V. Biller, K. N. Buck, K. W. Bruland, and K. A. Barbeau. 2014. Distinct pools of dissolved iron-binding ligands in the surface and benthic boundary layer of the California Current. Limnol. Oceanogr. **59**: 769–787. doi:10.4319/lo.2014.59.3.0769

Bundy, R. M., H. A. N. Abdulla, P. G. Hatcher, D. V. Biller, K. N. Buck, and K. A. Barbeau. 2015. Iron-binding ligands and humic substances in the San Francisco Bay estuary and estuarine-influenced shelf regions of coastal California. Mar. Chem. **173**: 183–194. doi:10.1016/j.marchem.2014.11.005

Bundy, R. M., R. M. Boiteau, C. McLean, K. A. Turk-Kubo, M. R. McIlvin, M. A. Saito, B. A. S. Van Mooy, and D. J. Repeta. 2018. Distinct siderophores contribute to iron cycling in the mesopelagic at station ALOHA. Front. Mar. Sci. **5**: 61, doi:10.3389/fmars.2018.00061

Burdige, D. J., W. M. Berelson, K. H. Coale, J. McManus, and K. S. Johnson. 1999. Fluxes of dissolved organic carbon from California continental margin sediments. Geochim. Cosmochim. Acta **63**: 1507–1515. doi:10.1016/S0016-7037(99)00066-6

Burdige, D. J., T. Komada, C. Magen, and J. P. Chanton. 2016. Modeling studies of dissolved organic matter cycling in Santa Barbara Basin (CA, USA) sediments. Geochim. Cosmochim. Acta **195**: 100–119. doi:10.1016/j.gca.2016.09.007

Capone, D. G., and D. A. Hutchins. 2013. Microbial biogeochemistry of coastal upwelling regimes in a changing ocean. Nat. Geosci. **6**: 711–717. doi:10.1038/ngeo1916

Chambers, M. C. and others 2012. A cross-platform toolkit for mass spectrometry and proteomics. Nat. Biotechnol. **30**: 918–920. doi:10.1038/nbt.2377

Checkley, D. M., and J. A. Barth. 2009. Patterns and processes in the California Current System. Prog. Oceanogr. **83**: 49–64. doi:10.1016/j.pocean.2009.07.028

Clark, C. D., L. P. Litz, and S. B. Grant. 2008. Salt marshes as a source of chromophoric dissolved organic matter (CDOM) to Southern California coastal waters. Limnol. Oceanogr. **53**: 1923–1933. doi:10.4319/lo.2008.53.5.1923

Deicke, M., J. F. Mohr, J.-P. Bellenger, and T. Wichard. 2014. Metallophore mapping in complex matrices by metal isotope coded profiling of organic ligands. Analyst **139**: 6096–6099. doi:10.1039/C4AN01461H

Elrod, V. A., W. M. Berelson, K. H. Coale, and K. S. Johnson. 2004. The flux of iron from continental shelf sediments: A missing source for global budgets. Geophys. Res. Lett. **31**: 2–5. doi:10.1029/2004GL020216

Elrod, V. A., K. S. Johnson, S. E. Fitzwater, and J. N. Plant. 2008. A long-term, high-resolution record of surface water iron concentrations in the upwelling-driven Central California region. J. Geophys. Res. Oceans **113**: 1–13. doi:10.1029/2007JC004610

Gledhill, M., P. McCormack, S. Ussher, E. P. Achterberg, R. F. C. Mantoura, and P. J. Worsfold. 2004. Production of siderophore type chelates by mixed bacterioplankton populations in nutrient enriched seawater incubations. Mar. Chem. **88**: 75–83. doi:10.1016/j.marchem.2004.03.003

Gledhill, M., and K. N. Buck. 2012. The organic complexation of iron in the marine environment: A review. Front. Microbiol. **3**: 1–17. doi:10.3389/fmicb.2012.00069

Hansell, D. A., N. R. Bates, and K. Gundersen. 1995. Mineralization of dissolved organic carbon in the Sargasso Sea. Mar. Chem. **51**: 201–212. doi:10.1016/0304-4203(95)00063-1

Hertkorn, N., M. Harir, K. M. Cawley, P. Schmitt-Kopplin, and R. Jaffé. 2015. Molecular characterization of dissolved organic matter from subtropical wetlands: A comparative study through the analysis of optical properties, NMR and FTICR/MS. Biogeosci. Discuss. **12**: 13711–13765. doi:10.5194/bgd-12-13711-2015

Hider, R. C., and X. Kong. 2010. Chemistry and biology of siderophores. Nat. Prod. Rep. **27**: 637–657. doi:10.1039/b906679a

Hopkinson, B. M., and K. A. Barbeau. 2012. Iron transporters in marine prokaryotic genomes and metagenomes. Environ. Microbiol. **14**: 114–128. doi:10.1111/j.1462-2920.2011.02539.x

Ito, Y., and A. Butler. 2005. Structure of synechobactins, new siderophores of the marine cyanobacterium *Synechococcus* sp. PCC 7002. Limnol. Oceanogr. **50**: 1918–1923. doi:10.4319/lo.2005.50.6.1918

John, S. G., J. Mendez, J. Moffett, and J. Adkins. 2012. The flux of iron and iron isotopes from San Pedro Basin sediments. Geochim. Cosmochim. Acta **93**: 14–29. doi:10.1016/j.gca.2012.06.003

Johnson, K. S., F. P. Chavez, and G. E. Friederich. 1999. Continental-shelf sediment as a primary source of iron for coastal phytoplankton. Nature **398**: 697–700.

Kem, M. P., H. K. Zane, S. D. Springer, J. M. Gauglitz, and A. Butler. 2014. Amphiphilic siderophore production by oil-associating microbes. Metallomics **6**: 1150–1155. doi:10.1039/c4mt00047a

Kim, S. and others 2016. PubChem substance and compound databases. Nucleic Acids Res. **44**: D1202–D1213. doi:10.1093/nar/gkv951

King, A. L., and K. Barbeau. 2007. Evidence for phytoplankton iron limitation in the southern California Current System. Mar. Ecol. Prog. Ser. **342**: 91–103. doi:10.3354/meps342091

King, A. L., and K. A. Barbeau. 2011. Dissolved iron and macronutrient distributions in the southern California Current System. J. Geophys. Res. **116**: 1–18. doi:10.1029/2010JC006324

King, A. L., S. A. Sañudo-Wilhelmy, P. W. Boyd, B. S. Twining, S. W. Wilhelm, C. Breene, M. J. Ellwood, and D. A. Hutchins. 2012. A comparison of biogenic iron quotas during a diatom spring bloom using multiple approaches. Biogeosciences **9**: 667–687. doi:10.5194/bg-9-667-2012

Laglera, L. M., and C. M. G. van den Berg. 2009. Evidence for geochemical control of iron by humic substances in seawater. Limnol. Oceanogr. **54**: 610–619. doi:10.4319/lo.2009.54.2.0610

Lohan, M. C., A. M. Aguilar-Islas, and K. W. Bruland. 2006. Direct determination of iron in acidified (pH 1.7) seawater samples by flow injection analysis with catalytic spectrophotometric detection: Application and intercomparison. Limnol. Oceanogr. **4**: 164–171. doi:10.4319/lom.2006.4.164

Lynn, R. J., and J. J. Simpson. 1987. The California Current System: The seasonal variability of its physical characteristics. J. Geophys. Res. Oceans **92**: 12947–12966. doi:10.1029/JC092iC12p12947

Macrellis, H. M., C. G. Trick, E. L. Rue, G. Smith, and K. W. Bruland. 2001. Collection and detection of natural iron-binding ligands from seawater. Mar. Chem. **76**: 175–187. doi:10.1016/S0304-4203(01)00061-5

Mahmood, A., M. M. Abualhaija, C. M. G. van den Berg, and S. G. Sander. 2015. Organic speciation of dissolved iron in estuarine and coastal waters at multiple analytical windows. Mar. Chem. **177**: 706–719. doi:10.1016/j.marchem.2015.11.001

Marchetti, A., and M. T. Maldonado. 2016. Iron, p. 233–279. *In* M. A. Borowitzka, J. Beardell, and J. Raven [eds.], The physiology of microalgae. Springer.

Martinez, J. S., J. N. Carter-Franklin, E. L. Mann, J. D. Martin, M. G. Haygood, and A. Butler. 2003. Structure and membrane affinity of a suite of amphiphilic siderophores produced by a marine bacterium. Proc. Natl. Acad. Sci. USA **100**: 3754–3759. doi:10.1073/pnas.0637444100

Mawji, E., M. Gledhill, J. A. Milton, G. A. Tarran, S. Ussher, A. Thompson, G. A. Wolff, P J. Worsfold, and E. P. Achterberg. 2008. Hydroxamate siderophores: Occurrence and importance in the Atlantic Ocean. Environ. Sci. Technol. **42**: 8675–8680. doi:10.1021/es801884r

Mawji, E., M. Gledhill, J. A. Milton, M. V. Zubkov, A. Thompson, G. A. Wolff, and E. P. Achterberg. 2011. Production of siderophore type chelates in Atlantic Ocean waters enriched with different carbon and nitrogen sources. Mar. Chem. **124**: 90–99. doi:10.1016/j.marchem.2010.12.005

Miethke, M., and M. A. Marahiel. 2007. Siderophore-based iron acquisition and pathogen control. Microbiol. Mol. Biol. Rev. **71**: 413–451. doi:10.1128/MMBR.00012-07

Morel, F. M. M., A. B. Kustka, and Y. Shaked. 2008. The role of unchelated Fe in the iron nutrition of phytoplankton. Limnol. Oceanogr. **53**: 400–404. doi:10.4319/lo.2008.53.1.0400

Parker, C. E., M. T. Brown, and K. W. Bruland. 2016. Scandium in the open ocean: A comparison with other group 3 trivalent metals. Geophys. Res. Lett. **43**: 2758–2764. doi:10.1002/2016GL067827

Parsons, T. R., Y. Maita, and C. M. Lalli. 1984. A manual of chemical and biological methods for seawater analysis. Pergamon Press.

Repeta, D. J. 2015. Chemical characterization and cycling of dissolved organic matter. *In* D. A. Hansell and C. A. Carlson [eds.], Biogeochemistry of marine dissolved organic matter. Elsevier. 22–58.

Rykaczewski, R. R., and D. M. Checkley. 2008. Influence of ocean winds on the pelagic ecosystem in upwelling regions. Proc. Natl. Acad. Sci. USA **105**: 1965–1970. doi:10.1073/pnas.0711777105

Sandy, M., and A. Butler. 2009. Microbial iron acquisition: Marine and terrestrial siderophores. Chem. Rev. **109**: 4580–4595. doi:10.1021/cr9002787

Strub, P. T., and C. James. 1995. The large-scale summer circulation of the California current. Geophys. Res. Lett. **22**: 207–210. doi:10.1029/94GL03011

Tunca, S., C. Barreiro, A. Sola-Landa, J. J. R. Coque, and J. F. Martın. 2007. Transcriptional regulation of the desferrioxamine gene cluster of *Streptomyces coelicolor* is mediated by binding of DmdR1 to an iron box in the promoter of the desA gene. FEBS J. **274**: 1110–1122. doi:10.1111/j.1742-4658.2007.05662.x

Vraspir, J. M., and A. Butler. 2009. Chemistry of marine ligands and siderophores. Ann. Rev. Mar. Sci. **1**: 43–63. doi:10.1146/annurev.marine.010908.163712

Wheatcroft, R. A., C. K. Sommerfield, D. E. Drake, J. C. Borgeld, and C. A. Nittrouer. 1997. Rapid and widespread

dispersal of flood sediment on the northern California margin. Geology **25**: 163–166. doi:10.1130/0091-7613(1997)025<0163:RAWDOF>2.3.CO;2

Xu, J. P., M. Noble, and S. L. Eittreim. 2002. Suspended sediment transport on the continental shelf near Davenport, California. Mar. Geol. **181**: 171–193. doi:10.1016/S0025-3227(01)00266-3

Acknowledgments

Thanks to Serena Dao and Geoffrey Smith for assistance with sample collection, Matt McIlvin for analytical assistance, and to the scientists and crew of the R/V *Melville.* We thank the Gordon and Betty Moore Foundation (Grant GBMF3298), the National Science Foundation (NSF) program in chemical oceanography (OCE-1356747, OCE-1259776, OCE-1736280), the NSF Science and Technology Center for Microbial Oceanography Research and Education (DBI-0424599), and the Simons Foundation (SCOPE Award 329,108) for support of this work. R. M. B was in part funded by a Linus Pauling Postdoctoral Fellowship at the Pacific Northwest National Laboratory (PNNL LDRD 69488), and J. N. F. was in part funded by a Rutgers Institute for Marine and Coastal Sciences Postdoctoral Fellowship.

Conflict of Interest

None declared.

Submitted 25 May 2018
Revised 22 June 2018
Accepted 30 August 2018

Associate editor: James Moffett